Sustainable Energy & Fuels

ROYAL SOCIETY OF CHEMISTRY

PAPER

View Article Online
View Journal | View Issue

Cite this: *Sustainable Energy Fuels*, 2025, **9**, 6173

Synthesis of jet fuel cycloalkane precursors with biomass-derived feedstocks over a bimetallic Cu–Ni catalyst

Anran Zhu,[abc] Zhufan Zou,[abc] Aiqin Wang,[abc] Yu Cong,[abc] Yinghua Yin[abc] and Ning Li *[abc]

2,5-Bis(furan-2-ylmethyl)cyclopentan-1-one (FCFDH), a C_{15} precursor for renewable jet fuel range cycloalkanes and high-value electronic photolithography material, was selectively synthesized *via* a cascade aldol condensation/hydrogenation reaction of furfural and cyclopentanone under solvent-free conditions. Non-noble metal Cu and Ni modified MgAl-hydrotalcite (Cu_2Ni_1/MgAl-HT) was found to be an effective and stable catalyst for this reaction. Under the optimized conditions (423 K, 4 MPa H_2, 10 h), 97.0% cyclopentanone conversion and 82.0% carbon yield of FCFDH were achieved. Based on the characterization results, the presence of Ni and Cu species increased the acidity of MgAl-HT and formed Ni–Cu alloy particles with an average size of 2.33 nm during the preparation of the catalyst. Both effects facilitate the aldol condensation of furfural and cyclopentanone and the formation of FCFDH by the selective hydrogenation of C=C bonds.

Received 25th June 2025
Accepted 12th September 2025

DOI: 10.1039/d5se00888c

rsc.li/sustainable-energy

Introduction

Due to the great social concern about sustainable development, the exploration and utilization of renewable energies have drawn a lot of attention. As the most abundant renewable carbon resource, biomass is a promising alternative for fossil energy in the production of fuels[1] and high-value chemicals.[2] Lignocellulose, which consists of cellulose, hemicellulose, and lignin, is particularly noteworthy due to its widespread availability, low cost, and carbon neutrality. Catalytic conversion is crucial for transforming lignocellulose into liquid fuels or specialty chemicals. This requires the development of efficient catalytic systems to optimize both the yield and selectivity of target products.

Furfural is an important platform compound that has been produced on an industrial scale through the hydrolysis and dehydration of hemicellulose.[3] After being hydrogenated under aqueous phase conditions, furfural can be selectively converted to cyclopentanone.[4] In the recent work of our group,[5] cyclopentanone was selectively synthesized by the hydrogenolysis of xylose or hemicellulose extracted from raw biomass. In some recent literature, jet fuel range C_{15} cycloalkane with high density and volumetric heat value was produced by the aldol condensation of cyclopentanone and furfural under the catalysis of NaOH,[6] MgO–ZrO_2,[7] KF/γ-Al_2O_3,[7] Na-$MgAlO_x$[8] or acidic resins,[9] followed by hydrodeoxygenation (HDO). Owing to the cyclic carbon chain structure, cycloalkanes exhibit inherent ring strain compared to linear alkanes. This structural character endows cycloalkanes with higher density and volumetric energy density than those of conventional fuels. These physicochemical properties are highly desirable for advanced, high-performance fuels. However, the products from the aldol condensation of cyclopentanone with one or two furfural molecule(s) (*i.e.* 2-(2-furylmethylidene)cyclopentanone (FC) and 2,5-bis(2-furylmethylidene)cyclopentanone (FCF)) in Scheme 1 are solids at room temperature. To facilitate mass transfer, organic solvents are used in the HDO step. In real application, this will lead to higher energy consumption and lower efficiency. 2,5-Bis(furan-2-ylmethyl)cyclopentan-1-one (FCFDH) is an important intermediate for the manufacturing of high-precision photosensitive materials used in the semiconductor industry.[10] In the conventional method, this compound can be produced by the selective hydrogenation of C=C bonds in FCF and exists in a liquid state at room temperature. In the recent work of Wang *et al.*,[11] a one-pot process was developed for the direct synthesis of FCFDH with furfural and cyclopentanone by cascade aldol condensation/hydrogenation under the co-catalysis of CaO and Pd/C. FCFDH as obtained exists as a liquid at room temperature. Therefore, it can be directly used for the subsequent HDO under solvent-free conditions. Taking into consideration high price and low reserves of Pd, it is still imperative to develop non-noble metal catalysts.

[a]*CAS Key Laboratory, of Science and Technology on Applied Catalysis, Dalian Institute of Chemical Physics, Chinese Academy of Sciences, Dalian 116023, China. E-mail: lining@dicp.ac.cn*

[b]*University of Chinese Academy of Sciences, 19 A Yuquan Road, Shijingshan District, Beijing 100049, China*

[c]*State Key Laboratory of Catalysis, Dalian Institute of Chemical Physics, Chinese Academy of Sciences, Dalian 116023, China*

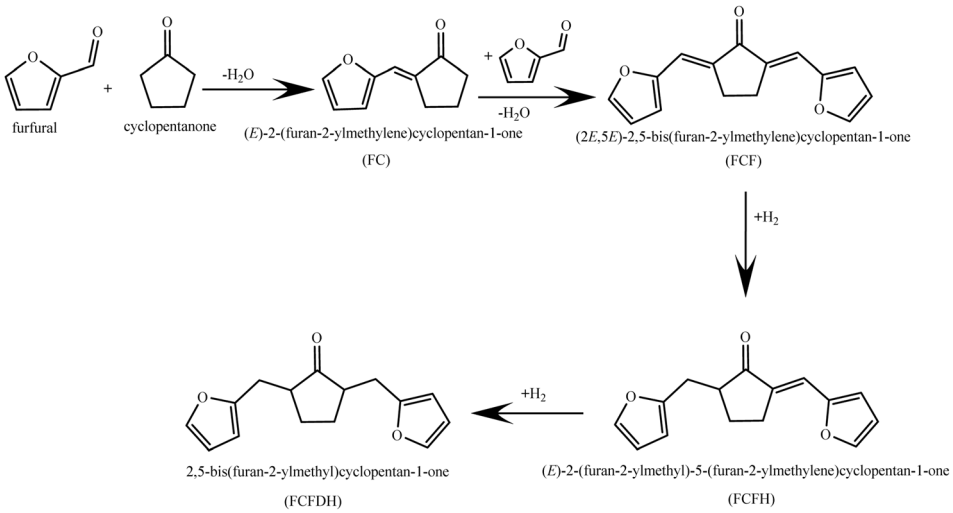

Scheme 1 Reaction route for the production of FCFDH from furfural and cyclopentanone.

In this work, non-noble metallic Cu and Ni modified MgAl-hydrotalcite (Cu_2Ni_1/MgAl-HT) was found to be an effective and stable catalyst for the direct synthesis of FCFDH by a cascade aldol condensation/hydrogenation reaction with furfural and cyclopentanone under solvent-free conditions. To get deeper insight into the effect of Cu and Ni species on the reaction, the catalysts were characterized by a series of technologies. This study provides a sustainable and green chemistry-compliant approach for synthesizing fuels or high-value-added chemicals using furfural and its derivatives.

Experimental

Chemicals

$Cu(NO_3)_2\cdot 3H_2O$, $Ni(NO_3)_2\cdot 6H_2O$, $Al(NO_3)_3\cdot 9H_2O$, $Mg(NO_3)_2\cdot 6H_2O$, Na_2CO_3 and NaOH used in this work were purchased from Aladdin Bio-Chem Technology Ltd.

Catalyst preparation

Cu and Ni modified MgAl-hydrotalcite catalysts (denoted as Cu_xNi_y/MgAl-HT, where x and y mean the theoretical atomic ratio of Cu and Ni) were prepared using a co-precipitation method. To facilitate the comparison, the total content of Cu and Ni in the catalyst was controlled at 5% by weight. Taking Cu_2Ni_1/MgAl-HT as an example, 50 mL of the aqueous solution containing 0.08 mol Na_2CO_3 and 0.12 mol NaOH was slowly added dropwise to another aqueous solution containing 0.04 mol $Mg(NO_3)_2\cdot 6H_2O$, 0.02 mol $Al(NO_3)_3\cdot 9H_2O$, 0.0014 mol $Cu(NO_3)_2\cdot 3H_2O$, and 0.0007 mol $Ni(NO_3)_2\cdot 6H_2O$ under vigorous stirring. The pH of the obtained mixture was adjusted to 10 using a 3 mol L^{-1} NaOH solution. The mixture was kept at 338 K for 24 h, and the resulting slurry was filtered, washed with deionized water until the pH was 7–8, and dried at 393 K for 12 h. Finally, the product was reduced at 773 K in a hydrogen flow (80 mL min^{-1}) for 4 h.

Characterization

X-ray diffraction (XRD) patterns of different catalysts were obtained using a PANalytical X'Pert-Pro powder X-ray diffractometer using Cu $K\alpha$ monochromatic radiation ($\lambda = 0.15418$ nm) at 40 V and 40 mA. N_2 physisorption of the catalysts was carried out using a Micromeritics ASAP 2010 apparatus. The elemental distribution of the catalysts was analyzed by scanning transmission electron microscopy (STEM) equipped with an energy dispersive X-ray spectroscopy (EDX) system. The basicity and acidity of the catalysts were characterized by CO_2-chemisorption, CO_2-TPD, NH_3-chemisorption and NH_3-TPD using a Micromeritics AutoChem 2910 chemisorption analyzer. Typically, 0.1 g of catalyst was used for each test. Prior to the measurement, the catalyst was pretreated under He flow at 423 K for 0.5 h to remove adsorbed moisture and impurities and then cooled to 353 K. After the baseline was stabilized, CO_2 (or NH_3) pulses were introduced until saturation adsorption was achieved. The adsorption signals were detected using a thermal conductivity detector (TCD), and the amounts of base (or acid) sites were calculated from the consumption of CO_2 (or NH_3). Subsequently, TPD experiments were carried out in the temperature range of 353–1173 K at a heating rate of 10 K min^{-1} under He flow, and the desorption profiles were monitored by mass spectrometry (m/z 44 for CO_2 and m/z 15 for NH_3). The thermogravimetric–mass spectrometry (TG-MS) data of the catalyst were obtained using a TA Instruments SDT Q600 system coupled with an InProgress Instruments GAM 200 mass spectrometer (MS). For each measurement, 0.1 g of catalyst was loaded into the sample pan. The analyses were carried out under a flowing 20% O_2/N_2 mixture at a flow rate of 100 mL min^{-1}. During the test, the sample temperature was increased from 303 K to 1073 K at a heating rate of 10 K min^{-1}.

Activity test

Activity tests were carried out in a 50 mL stainless-steel batch reactor (Parr 5513 Stainless Steel, Parr Instrument). For each

test, 10 mmol cyclopentanone, 20 mmol furfural, and 0.05 g catalysts were used. Before the tests, the reactor was purged with nitrogen three times and charged with hydrogen to 4 MPa. The reaction mass was heated at 423 K under stirring (at a rotation speed of 500 rpm) for 10 h and quenched to room temperature with cool water. The product was dissolved in 20 mL dichloromethane containing the internal standard of tridecane. The liquid products were analyzed using an Agilent 7890A gas chromatograph.

Conversion of the substrate (%) = (number of moles of the substrate consumed during activity test)/(number of moles of the substrate in the feedstock) × 100%.

Carbon yield of specific product (%) = (number of moles of carbon in the specific product obtained in the activity test)/(number of moles of carbon in the feedstock) × 100%.

Results and discussion

MgAl-HT is a solid base catalyst that was often used in the aldol condensation of biomass derived carbonyl compounds.[12] In this work, it was reported for the first time that the modification of the MgAl-HT catalyst with a small amount of Cu or Ni species could significantly increase its activity for the condensation of furfural and cyclopentanone under a hydrogen atmosphere (see Fig. 1a and S1–S5). Based on the analysis of products (see Fig. 1b and Fig. S1–S5 in the SI), this phenomenon may be rationalized because the presence of Ni or Cu promoted the C=C bond in the FCF generated from the aldol condensation of furfural and cyclopentanone. As we know, aldol condensation is a reversible reaction. From the point of view of reaction equilibrium, the saturation of C=C bonds in FCF can prevent retro aldol condensation. This could be one reason for the higher yields of C_{15} oxygenates over the Cu/MgAl-HT and Ni/MgAl-HT catalysts. However, the carbon yields of FCFDH over the Cu/MgAl-HT and Ni/MgAl-HT catalysts were unsatisfactory.

When we used bimetallic CuNi/MgAl-HT as the catalyst, evidently higher yields of FCFDH were achieved under the same reaction conditions (see Fig. 1a; the carbon balances are shown in Fig. S6). The advantage of the bimetallic catalyst is more evident when we use Cu_2Ni_1/MgAl-HT as the catalyst (see Fig. 1b). Over it, higher total yields of C_{15} and C_{10} oxygenates and lower yield of cyclopentanol than those over the other two bimetallic CuNi/MgAl-HT catalysts were achieved under the investigated reaction conditions. This is advantageous in real application. This phenomenon can be explained by the higher activity of the Cu_2Ni_1/MgAl-HT catalyst for the hydrogenation of C=C bonds in the FCF generated from the aldol condensation of furfural and cyclopentanone. As we know, the C_{15} and C_{10} oxygenates obtained in this work can be converted to jet fuel range C_{15} and C_{10} cycloalkanes. In contrast, the cyclopentane from the hydrodeoxygenation of cyclopentanol has a low boiling point. Therefore, it can't be blended into jet fuel.

To gain deeper insight into the excellent performance of Cu_2Ni_1/MgAl-HT, we characterized catalysts by a series of technologies. Based on the XRD patterns shown in Fig. 2 and 3, the precursors of Ni/MgAl-HT, Cu/MgAl-HT and Cu_xNi_y/MgAl-HT exhibited typical diffraction patterns at 2θ angles of 11.7°,

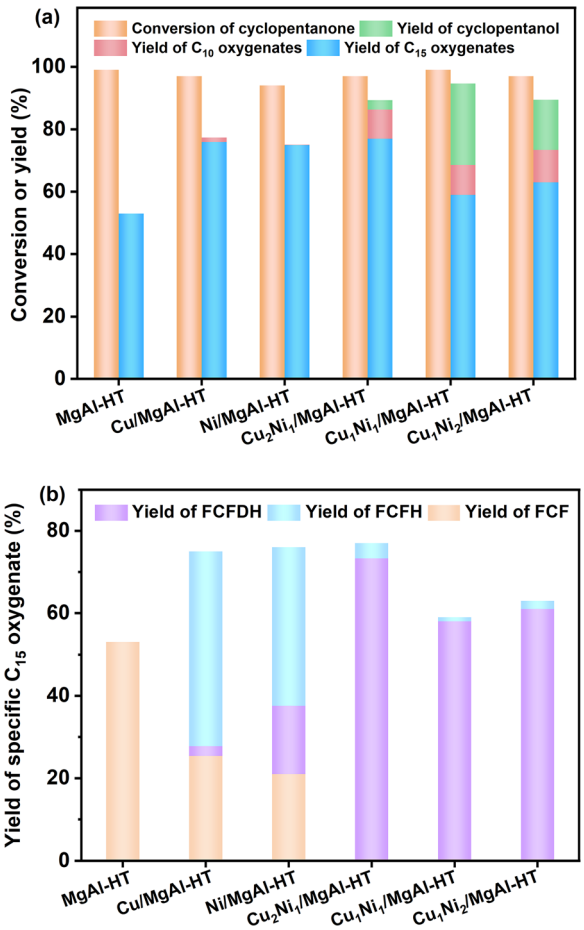

Fig. 1 (a) Conversions of cyclopentanone and the yields of different products, and (b) the yield of the specific C_{15} oxygenate over different catalysts. Reaction conditions: 423 K, 4 MPa H_2, 10 h; 10 mmol cyclopentanone, 20 mmol furfural and 0.05 g catalyst were used in each test.

23.4°, 34.5°, 39.6°, 60.7° and 62.2°, corresponding to the (003), (006), (012), (015), (018), (110) and (113) planes of LDHs (PDF #00-056-0956), respectively. Upon calcination at 773 K, the

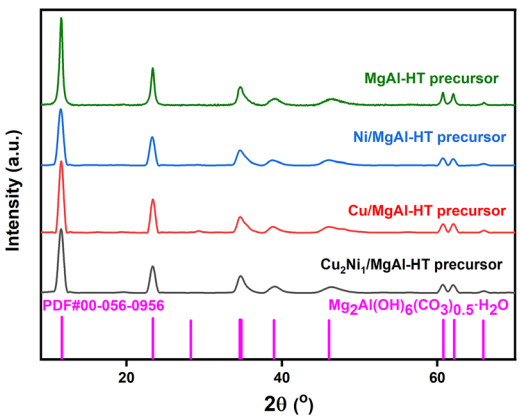

Fig. 2 XRD patterns of the MgAl-HT, Ni/MgAl-HT, Cu/MgAl-HT and Cu_2Ni_1/MgAl-HT catalyst precursors.

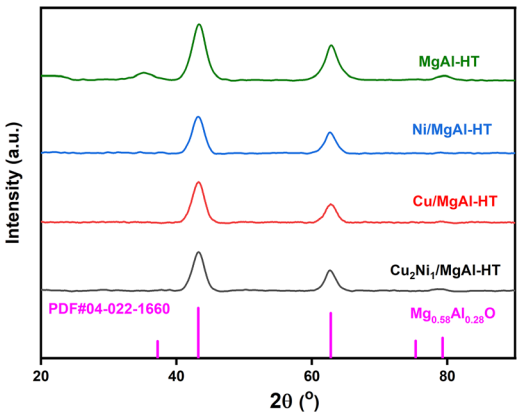

Fig. 3 XRD patterns of the MgAl-HT, Ni/MgAl-HT, Cu/MgAl-HT and Cu_2Ni_1/MgAl-HT catalysts.

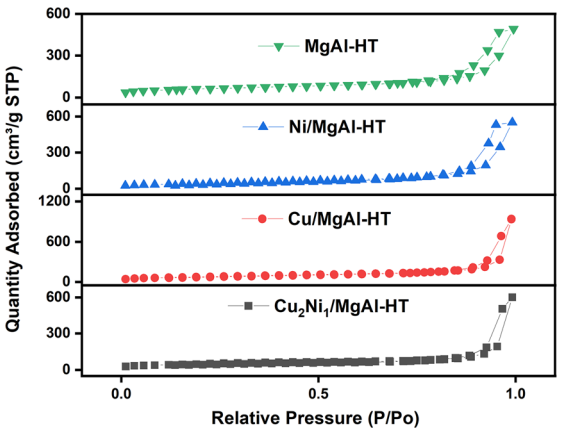

Fig. 4 N_2 adsorption–desorption isotherms of the MgAl-HT, Ni/MgAl-HT, Cu/MgAl-HT and Cu_2Ni_1/MgAl-HT catalysts.

structure of LDHs collapsed and converted to their corresponding highly dispersed mixed oxides. After the reduction at 773 K, major diffraction peaks at 2θ angles of 37.2°, 43.2° and 62.8° were observed. These peaks can be assigned to the (111), (200) and (220) planes of $Mg_{0.58}Al_{0.28}O$ (PDF #04-022-1660). No diffraction peaks corresponding to Cu or Ni species were observed, indicating that Cu and Ni species are highly dispersed on the surfaces of catalysts.

Subsequently, we also characterized the catalysts by N_2-physisorption. As shown in Fig. 4 and Table 1, the N_2 adsorption–desorption isotherms of the catalysts exhibit a distinct hysteresis loop, characteristic of a type IV isotherm, indicating the presence of abundant mesoporous structures.[8] It is worth mentioning that the Cu_2Ni_1/MgAl-HT catalyst has evidently higher specific BET surface area (592 $m^2\ g^{-1}$) than those of Cu/MgAl-HT (275 $m^2\ g^{-1}$) and Ni/MgAl-HT (162 $m^2\ g^{-1}$), which may be one reason for the higher activity of the Cu_2Ni_1/MgAl-HT catalyst for the hydrogenation of C=C bonds.

The Cu_2Ni_1/MgAl-HT catalyst was also characterized by TEM. As shown in Fig. 5a, the precursor of the Cu_2Ni_1/MgAl-HT catalyst exhibits a layered double hydroxide. This is consistent

Table 1 Specific BET surface areas (S_{BET}), the pore volumes (V_t) and average pore sizes of MgAl-HT, Ni/MgAl-HT, Cu/MgAl-HT and Cu_2Ni_1/MgAl-HT catalysts

Catalyst	S_{BET} ($m^2\ g^{-1}$)	V_t ($cm^3\ g^{-1}$)	Average pore size (nm)
MgAl-HT	211	0.69	17.4
Ni/MgAl-HT	162	0.82	18.2
Cu/MgAl-HT	275	0.84	22.2
Cu_2Ni_1/MgAl-HT	592	1.91	20.9

with the LDH structure confirmed by the XRD results. As shown in Fig. 5e and S7–S8, elemental mapping reveals that Mg, Al, Cu, and Ni species are highly dispersed. The elemental composition closely matches the theoretical values and the ones measured by ICP-OES analysis (Cu content: 2.9 wt%; Ni content: 1.3 wt%). After the reduction with hydrogen, the LDH framework collapsed and transformed into a mixed oxide phase. Remarkably, the MgAl-HT support effectively inhibited the sintering of metal particles, preserving high dispersion of metal nanoparticles with an average size of 2.33 nm (Fig. 5b). As shown in Fig. 5f, elemental mapping further validated the uniform distribution of metallic species. As shown in Fig. 5c and d, isolated Ni nanoparticles displayed a lattice spacing of 0.202 nm, corresponding to the (111) plane of metallic Ni. Cu particles exhibited a characteristic (111) spacing of 0.208 nm. Bimetallic CuNi alloy domains were identified *via* a distinct (111) lattice spacing of 0.207 nm, intermediate between pure Cu and Ni values. The MgAl-HT support has a (200) plane spacing of 0.209 nm, matching the XRD reference (PDF #04-022-1660). Besides, the MgAl-HT support and Ni (or Cu) species closely interacted, forming a homogeneous boundary due to their close ionic radius and lattice matching between the (200) plane of $Mg_{0.58}Al_{0.28}O$ and (111) plane of Ni/Cu ($Mg_{0.58}Al_{0.28}O$: 0.209 nm, Ni: 0.202 nm, and Cu: 0.208 nm). In Fig. 5d, the Cu and Ni species were not directly observed. We believe that the majority of Cu species on the Cu_2Ni_1/MgAl-HT catalyst are strongly bound to either Ni or the MgAl-HT support, forming a dilute CuNi alloy and Cu-modified MgAlO species. The strong interaction between the CuNi alloy particles and MgAl-HT support, driven by their similar ionic radii and lattice matching, creates a homogeneous boundary that inhibits metal particle aggregation, thus maintaining high activity in the hydrogenation of C=C bonds.

To discriminate the chemical states of Cu and/or Ni species, the catalysts were characterized by XPS (see Fig. S9). In the Cu 2p spectra (see Fig. 6a and d), four distinct peaks were resolved at about 955.24 eV, 952.57 eV, 934.34 eV and 932.73 eV. These peaks can be attributed to the Cu $2p_{1/2}$ and Cu $2p_{3/2}$ signals of Cu^{2+}, Cu^0 or Cu^+ species, respectively.[13] The Cu^{2+} satellite peaks were also observed at around 945 eV. Fig. 6b and e illustrated the Cu LMM Auger electron spectra that were used to distinguish Cu^0 and Cu^+ by deconvoluting the broad signal into two overlapping peaks at 916.40 eV and 909.40 eV, referring to Cu^0 and Cu^+ species, respectively.[13] Based on the normalized areas of the corresponding featured peaks, the individual contents of

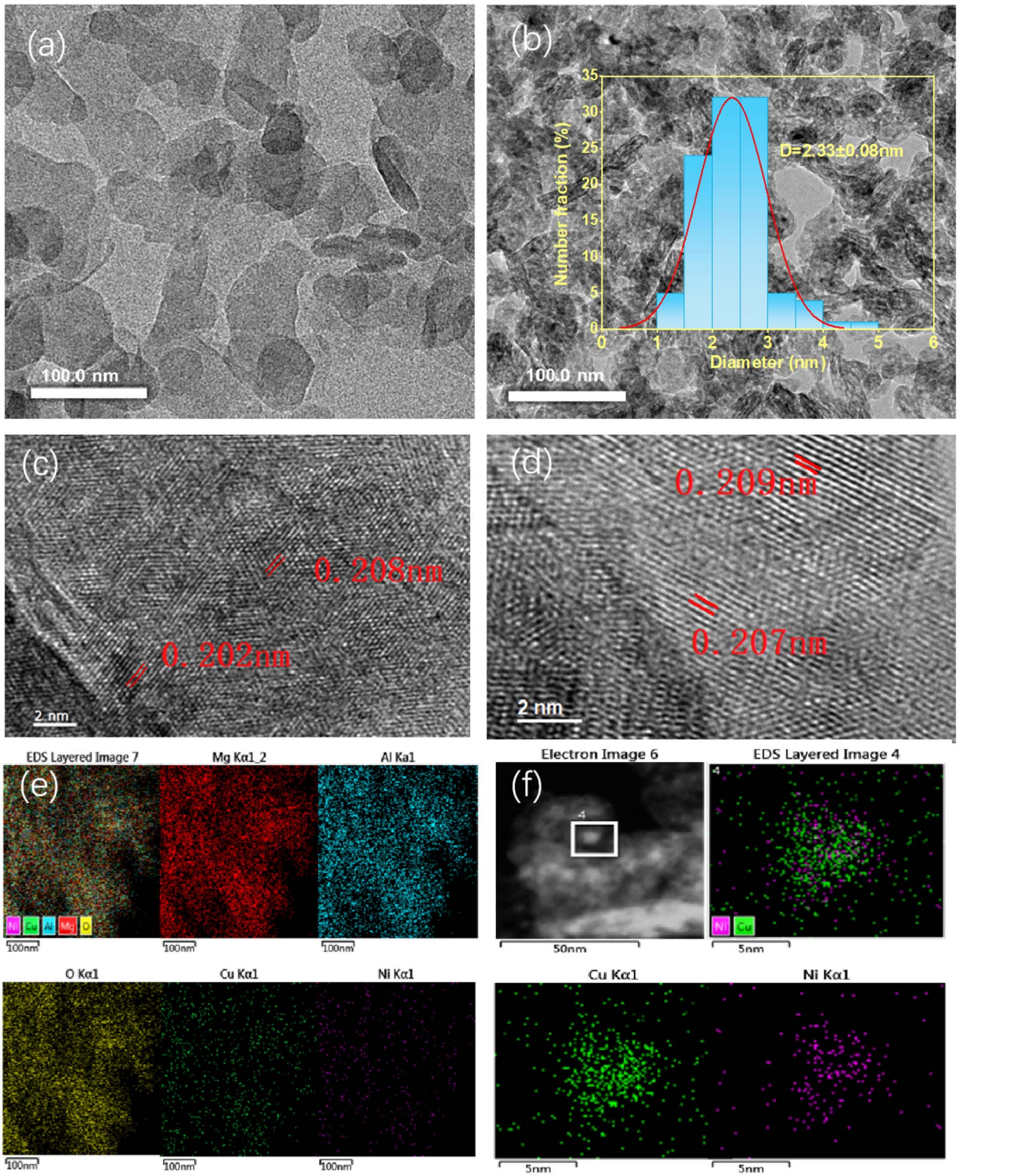

Fig. 5 TEM images and the EDS elemental mapping of the Cu_2Ni_1/MgAl-HT precursors (a, c and e) and the Cu_2Ni_1/MgAl-HT catalyst (b, d and f).

Cu species with different valence states were quantified. The percentages of Cu^0, Cu^+, and Cu^{2+} species are summarized in Table 2. Based on Fig. 6b and e, the Cu_2Ni_1/MgAl-HT and Cu/MgAl-HT contain Cu in three different oxidation states. The introduction of Ni species significantly increases the proportion of Cu^0 and Cu^+ on the catalyst surface. For the Cu_2Ni_1/MgAl-HT catalyst, approximately 25% of the Cu^{2+} species has strong interaction with Mg^{2+} or Ni^{2+} species, which makes them resistant to reduction under the given conditions, or from the surface reoxidation of metallic Cu particles during *ex situ* measurements. Meanwhile, around 40% of Cu species exist as Cu^0, which are almost atomically dispersed in the presence of

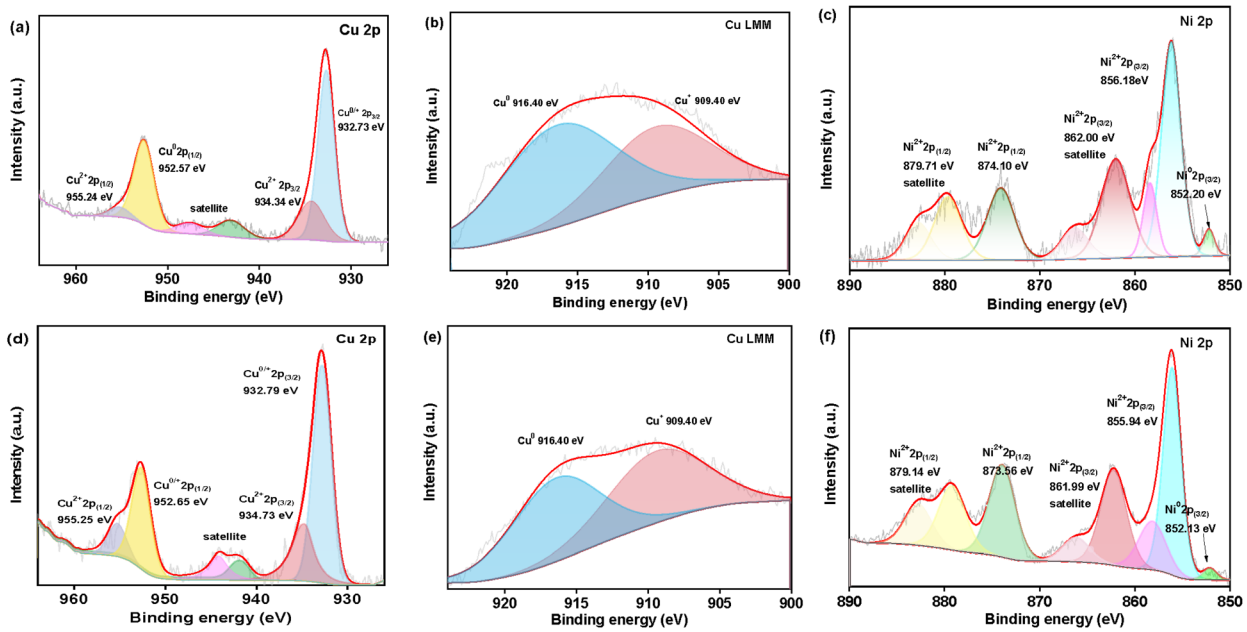

Fig. 6 XPS spectra of (a–c) Cu 2p, Cu-LMM, and Ni 2p for Cu_2Ni_1/MgAl-HT, (d and e) Cu 2p and Cu-LMM for Cu/MgAl-HT, and (f) Ni 2p for Ni/MgAl-HT catalysts.

Table 2 Surface atomic percentages of different Cu species and O species over the Ni/MgAl-HT, Cu/MgAl-HT, and Cu_2Ni_1/MgAl-HT catalysts, as determined from the normalized peak areas in the XPS spectra

	Surface atomic percentages of different Cu species (%)			Surface atomic percentages of different O species (%)	
Catalyst	Cu^0	Cu^+	Cu^{2+}	O_{latt}	O_{ads}
Ni/MgAl-HT	—	—	—	29.4	70.6
Cu/MgAl-HT	29.9	33.4	36.7	45.2	54.8
Cu_2Ni_1/MgAl-HT	39.9	34.4	25.7	43.5	56.5

metallic Ni. The remaining 35% of Cu species are present as Cu^+, predominantly located at the interface between Cu^0 and Cu^{2+}/Mg^{2+}.

As shown in Fig. 6c, five peaks at 879.71 eV, 874.10 eV, 862.00 eV, 856.18 eV and 852.20 eV were detected in the Ni 2p spectra of the Cu_2Ni_1/MgAl catalyst. According to the literature,[14] these peaks should be ascribed to the Ni $2p_{1/2}$ satellite peak, Ni^{2+} $2p_{1/2}$, Ni $2p_{3/2}$ satellite peak, Ni^{2+} $2p_{3/2}$ and Ni^0 $2p_{3/2}$, respectively. Accordingly, the Ni^{2+} and Ni^0 species were concomitant on the surface of all samples. A certain amount of Ni^{2+} species originated either from the encapsulation effect, where Ni species interacted strongly with $MgO(Al_2O_3)$ and were hardly reduced to metallic Ni, or from the surface reoxidation of metallic Ni particles during the *ex situ* measurements.

Compared with the Ni/MgAl-HT catalyst, the Ni $2p_1/_2$ and $2p_3/_2$ signals of the Cu_2Ni_1/MgAl-HT catalyst shift to higher binding energies (see Fig. 6f). In contrast, the Cu $2p_1/_2$ and $2p_3/_2$ signals of Cu_2Ni_1/MgAl-HT shift to lower binding energies (see Fig. 6a and d). These observations suggest that there is a strong interaction between the Cu and Ni species in the Cu_2Ni_1/MgAl-HT catalyst, leading to the transfer of electrons from Ni to Cu. The introduction of Ni effectively modulates the valence state distribution of Cu species, enhancing the ability to dissociate H_2, thereby improving hydrogenation activity. Additionally, it optimizes the interaction between Cu^+ and Cu^{2+}, refining the interfacial structure to facilitate hydrogen activation and transfer. These Cu species act as a dynamic reservoir for hydrogen adsorption/desorption processes, thereby promoting efficient hydrogen transfer. This optimization not only enhances hydrogen mobility on the catalyst surface but also improves the stability of Cu species, reducing the risk of sintering or deactivation.[15]

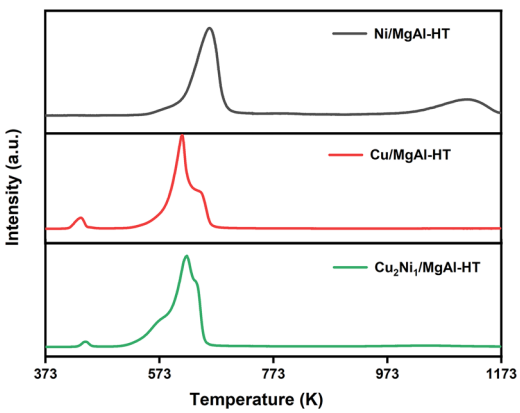

Fig. 7 H_2-TPR profiles of the Ni/MgAl-HT, Cu/MgAl-HT and Cu_2Ni_1/MgAl-HT catalysts.

Table 3 Base site and acid site concentrations of the investigated catalysts measured by CO_2-chemisorption and NH_3-chemisorption

Catalyst	Base site concentration ($\mu mol\ g^{-1}$)	Acid site concentration ($\mu mol\ g^{-1}$)
MgAl-HT	111.7	51.2
Ni/MgAl-HT	54.6	187.2
Cu/MgAl-HT	87.1	177.2
Cu_2Ni_1/MgAl-HT	64.3	260.9

As shown in Fig. S10 and Table 2, the O 1s core level depicted two distinct peaks at 530.7 eV and 532.4 eV, which should be assigned to strong base sites of lattice oxygen (O_{latt}) and weak base sites of adsorbed oxygen, respectively. Compared with the Ni/MgAl-HT catalyst, the percentage of O_{latt} in the Cu_2Ni_1/MgAl-HT catalyst was evidently higher (43.5% *vs.* 29.4%). This can be rationalized because the dehydration of hydroxyl oxygen in the presence of Cu species increased the strength of base sites for condensation reactions.[16]

Based on the H_2-TPR profiles shown in Fig. 7, the reduction temperature of the Cu_2Ni_1/MgAl-HT catalyst is higher than that of the Cu/MgAl-HT catalyst. Meanwhile, it is also lower than that of the Ni/MgAl-HT catalyst. These results further confirm the strong interactions between Cu and Ni species in the Cu_2Ni_1/MgAl-HT system. The H_2-TPR profiles of Cu_2Ni_1/MgAl-HT and Cu/MgAl-HT catalysts reveal two main reduction peaks. The peak at around 443 K corresponds to the reduction of highly dispersed CuO nanoparticles to Cu^0, while the peak at around 620 K represents the reduction of larger CuO particles. Compared with the Cu/MgAl-HT catalyst, the peak at around 620 K in the profile of the Cu_2Ni_1/MgAl-HT catalyst shifts to a higher temperature, which indicates that the presence of Ni decreases the reducibility of Cu species.

Furthermore, we also studied the basicity and acidity of the MgAl-HT, Cu/MgAl-HT, Ni/MgAl-HT and Cu_2Ni_1/MgAl-HT catalysts by CO_2-chemisorption and NH_3-chemisorption. From the results illustrated in Table 3, the base site concentrations of Cu/MgAl-HT, Ni/MgAl-HT and Cu_2Ni_1/MgAl-HT are lower than that of MgAl-HT. However, the acid site concentrations of Cu/MgAl-HT, Ni/MgAl-HT and Cu_2Ni_1/MgAl-HT are higher than that of MgAl-HT. This phenomenon is more evident for Cu_2Ni_1/MgAl-HT. In the previous work of Corma *et al.*,[17] it was suggested that acid sites can activate the carbonyl group by polarizing the C=O bond and make the carbonyl group more electrophilic, which is favorable in aldol condensation. Based on these results, we believe that the relatively higher acidity of Cu_2Ni_1/MgAl-HT may be one reason for its excellent performance in the condensation of furfural and cyclopentanone. We also characterized these catalysts by CO_2-TPD and NH_3-TPD. Based on the results illustrated in Fig. S11 and S12, no evident relationship was observed between the base strength (or acid strength) and their performance in the condensation of furfural and cyclopentanone.

After further optimization of reaction temperature and reaction time (see Fig. 8, 9 and S13–S14), 82.0% carbon yield of FCFDH was achieved over the Cu_2Ni/MgAl-HT catalyst after the reaction was carried out at 423 K, 4 MPa H_2 for 10 h. Taking into account the cyclopentanone conversion and the selectivity of FCFDH in the products, we believe that they are the optimal reaction conditions for the production of FCFDH over the Cu_2Ni/MgAl-HT catalyst. It was worth mentioning that the activity of the Cu2Ni/MgAl-HT catalyst decreased after it was used in the activity test (see Fig. S16). According to the results of N_2-physisorption and CO_2-chemisorption (see Table S1), evident decreases in the specific BET surface area, pore volume, average pore size and the amount of base sites were observed after the Cu_2Ni_1/MgAl-HT catalyst was used for the activity test, which may be the reason for the lower activity of the spent Cu_2Ni/MgAl-HT catalyst. Based on thermogravimetric analysis (TGA) of the used Cu_2Ni_1/MgAl-HT catalyst (see Fig. S17), these results can be rationalized by the carbon deposition generated during the reaction. As we know, furfural has high reactivity. Under the investigated conditions, it can be converted to furoic acid and furfuryl alcohol by the Cannizzaro reaction. These compounds may react with base sites or form a polymer on the

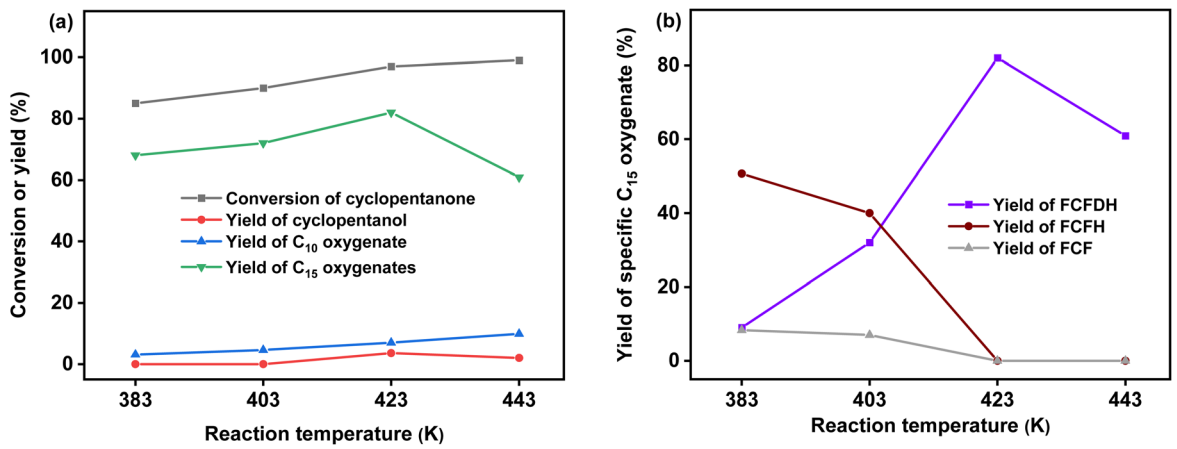

Fig. 8 (a) Conversions of cyclopentanone and the yields of different products, and (b) yield of the specific C_{15} oxygenate over the Cu_2Ni_1/MgAl-HT catalyst as a function of reaction temperature. Reaction conditions: 4 MPa H_2, 10 h; 10 mmol cyclopentanone, 20 mmol furfural, and 0.05 g Cu_2Ni_1/MgAl-HT catalyst were used in each test.

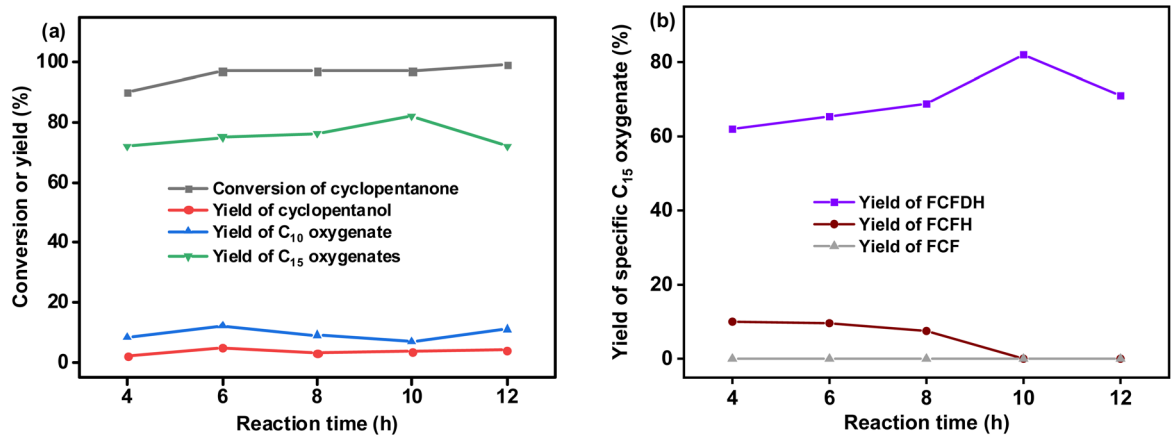

Fig. 9 (a) Conversions of cyclopentanone and the yields of different products, and (b) yield of the specific C_{15} oxygenate over the Cu_2Ni_1/MgAl-HT catalyst as a function of reaction time. Reaction conditions: 423 K, 4 MPa H_2; 10 mmol cyclopentanone, 20 mmol furfural, and 0.05 g Cu_2Ni_1/MgAl-HT catalyst were used in each test.

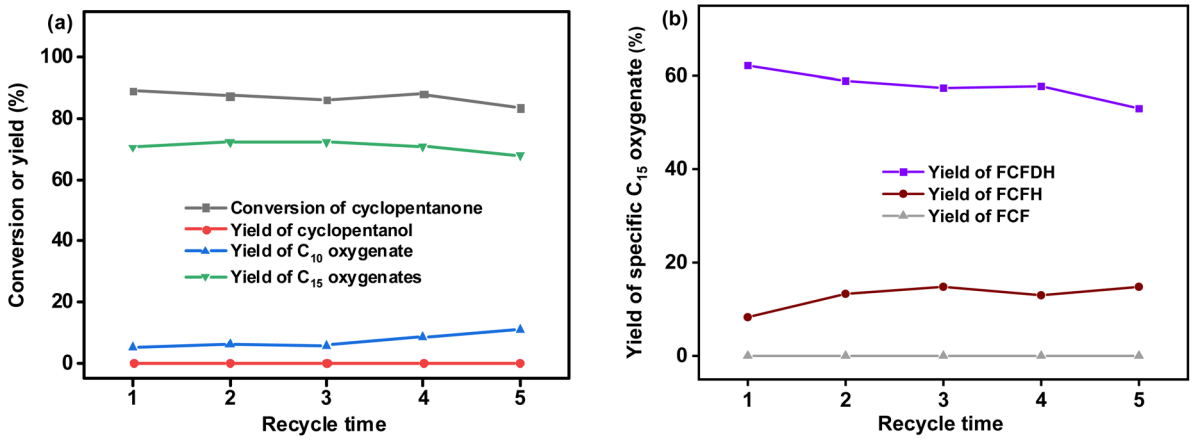

Fig. 10 (a) Conversions of cyclopentanone and the yields of different products, and (b) yield of the specific C_{15} oxygenate over the Cu_2Ni_1/MgAl-HT catalyst as a function of recycle time. Reaction conditions: 423 K, 4 MPa H_2, 1 h; 10 mmol cyclopentanone, 20 mmol furfural, and 0.05 g Cu_2Ni_1/MgAl-HT catalyst were used in each test.

surface of the Cu_2Ni/MgAl-HT catalyst, which may be the reason for the carbon deposition. As a solution to this problem, it was found that the Cu_2Ni/MgAl-HT catalyst can be regenerated by calcination and reduction (see Fig. 10 and S15). To fulfil the need of real application, we also checked the reusability of the Cu_2Ni/MgAl-HT catalyst. After each usage, the catalyst was thoroughly washed with methanol, calcined in air at 737 K for 2 h and reduced in a hydrogen flow at 773 K for 4 h. As we expected, the Cu_2Ni/MgAl-HT catalyst was stable under the investigated conditions. No significant change in catalytic performance was observed during the five repeated usages (see Fig. 10). Taking into consideration the high activity, good reusability, and low cost of Cu_2Ni_1/MgAl-HT, we think that it is a promising catalyst for future application.

Conclusions

A bimetallic Cu_2Ni_1/MgAl-HT catalyst demonstrated excellent activity and stability for the direct synthesis of FCFDH by the cascade aldol condensation/hydrogenation reaction of furfural and cyclopentanone that can be derived from lignocellulose. Under optimized conditions (423 K, 4 MPa H_2, 10 h), high cyclopentanone conversion and good yield of FCFDH were achieved over the Cu_2Ni_1/MgAl-HT catalyst. Based on the characterization results, the introduction of Ni species led to the formation of CuNi alloy sites due to their similar ionic radii and lattice matching, which is favorable for the selective hydrogenation of C=C bonds in the FCF generated from the aldol condensation of furfural and cyclopentanone. Moreover, the modification of MgAl-HT with Cu and Ni also increased its acidity. Both effects led to the good performance of the Cu_2Ni_1/MgAl-HT catalyst for the direct synthesis of FCFDH with furfural and cyclopentanone under the investigated conditions. This study provides valuable insights into the synthesis of jet-fuel precursors from furfural and cyclopentanone with non-noble metal bifunctional catalysts.

Conflicts of interest

There are no conflicts to declare.

Data availability

The data supporting this article have been included as part of the SI. Supplementary information: gas chromatograms, ^{1}H NMR and ^{13}C NMR spectra and carbon balances of the products; characterization results of catalysts; a comparison of the catalytic performance and physicochemical properties between the fresh and spent Cu_2Ni_1/MgAl-HT catalysts. See DOI: **https://doi.org/10.1039/d5se00888c**.

Acknowledgements

This work was supported by the National Key R&D Program of China (no. 2022YFB4201802), National Natural Science Foundation of China (no. 22178335) and DICP (Grant: DICP I202448).

Notes and references

1 (*a*) G. W. Huber, S. Iborra and A. Corma, *Chem. Rev.*, 2006, **106**, 4044–4098; (*b*) G. Li, R. Wang, J. Pang, A. Wang, N. Li and T. Zhang, *Chem. Rev.*, 2024, **124**, 2889–2954; (*c*) G. W. Huber, J. N. Chheda, C. J. Barrett and J. A. Dumesic, *Science*, 2005, **308**, 1446–1450; (*d*) E. L. Kunkes, D. A. Simonetti, R. M. West, J. C. Serrano-Ruiz, C. A. Gartner and J. A. Dumesic, *Science*, 2008, **322**, 417–421; (*e*) B. G. Harvey and R. L. Quintana, *Energy Environ. Sci.*, 2010, **3**, 352–357; (*f*) A. Corma, O. de la Torre, M. Renz and N. Villandier, *Angew. Chem., Int. Ed.*, 2011, **50**, 2375–2378; (*g*) P. Anbarasan, Z. C. Baer, S. Sreekumar, E. Gross, J. B. Binder, H. W. Blanch, D. S. Clark and F. D. Toste, *Nature*, 2012, **491**, 235–239; (*h*) A. Corma, O. de la Torre and M. Renz, *Energy Environ. Sci.*, 2012, **5**, 6328–6344; (*i*) J. Q. Bond, A. A. Upadhye, H. Olcay, G. A. Tompsett, J. Jae, R. Xing, D. M. Alonso, D. Wang, T. Zhang, R. Kumar, A. Foster, S. M. Sen, C. T. Maravelias, R. Malina, S. R. H. Barrett, R. Lobo, C. E. Wyman, J. A. Dumesic and G. W. Huber, *Energy Environ. Sci.*, 2014, **7**, 1500–1523; (*j*) Q.-N. Xia, Q. Cuan, X.-H. Liu, X.-Q. Gong, G.-Z. Lu and Y.-Q. Wang, *Angew. Chem., Int. Ed.*, 2014, **53**, 9755–9760; (*k*) Q. Xia, Z. Chen, Y. Shao, X. Gong, H. Wang, X. Liu, S. F. Parker, X. Han, S. Yang and Y. Wang, *Nat. Commun.*, 2016, **7**, 11162.

2 (*a*) M. J. Climent, A. Corma and S. Iborra, *Chem. Rev.*, 2011, **111**, 1072–1133; (*b*) A. Wang and T. Zhang, *Acc. Chem. Res.*, 2013, **46**, 1377–461386; (*c*) C. Li, X. Zhao, A. Wang, G. W. Huber and T. Zhang, *Chem. Rev.*, 2015, **115**, 11559–11624; (*d*) S. Shylesh, A. A. Gokhale, C. R. Ho and A. T. Bell, *Acc. Chem. Res.*, 2017, **50**, 2589–2597; (*e*) C. Luo, S. Wang and H. Liu, *Angew. Chem., Int. Ed.*, 2007, **46**, 7636–7639; (*f*) H. Liu, T. Jiang, B. Han, S. Liang and Y. Zhou, *Science*, 2009, **326**, 1250–1252; (*g*) T. P. Vispute, H. Y. Zhang, A. Sanna, R. Xiao and G. W. Huber, *Science*, 2010, **330**, 1222–1227; (*h*) Y. Liu, C. Luo and H. C. Liu, *Angew. Chem., Int. Ed.*, 2012, **51**, 3249–3253; (*i*) Y. L. Wang, W. P. Deng, B. J. Wang, Q. H. Zhang, X. Y. Wan, Z. C. Tang, Y. Wang, C. Zhu, Z. X. Cao, G. C. Wang and H. L. Wan, *Nat. Commun.*, 2013, **4**, 2141; (*j*) W. Deng, Y. Wang, S. Zhang, K. M. Gupta, M. J. Hülsey, H. Asakura, L. Liu, Y. Han, E. M. Karp, G. T. Beckham, P. J. Dyson, J. Jiang, T. Tanaka, Y. Wang and N. Yan, *Proc. Natl. Acad. Sci. U.S.A.*, 2018, **115**, 5093–5098; (*k*) W. Deng, L. Yan, B. Wang, Q. Zhang, H. Song, S. Wang, Q. Zhang and Y. Wang, *Angew. Chem., Int. Ed.*, 2021, **60**, 4712–4719; (*l*) Q. Meng, J. Yan, R. Wu, H. Liu, Y. Sun, N. Wu, J. Xiang, L. Zheng, J. Zhang and B. Han, *Nat. Commun.*, 2021, **12**, 4534; (*m*) K. Zhang, Q. Meng, H. Wu, J. Yan, X. Mei, P. An, L. Zheng, J. Zhang, M. He and B. Han, *J. Am. Chem. Soc.*, 2022, **144**, 20834–20846; (*n*) A. Osatiashtiani, A. F. Lee, D. R. Brown, J. A. Melero, G. Morales and K. Wilson, *Catal. Sci. Technol.*, 2014, **4**, 333–342; (*o*) M. T. Reche, A. Osatiashtiani, L. J. Durndell, M. A. Isaacs, A. Silva, A. F. Lee and K. Wilson, *Catal. Sci. Technol.*, 2016, **6**, 7334–7341.

3 J.-P. Lange, E. van der Heide, J. van Buijtenen and R. Price, *ChemSusChem*, 2012, **5**, 150–166.

4 (*a*) M. Hronec and K. Fulajtarova, *Catal. Commun.*, 2012, **24**, 100–104; (*b*) R. Fang, H. Liu, R. Luque and Y. Li, *Green Chem.*, 2015, **17**, 4183–4188; (*c*) X.-L. Li, J. Deng, J. Shi, T. Pan, C.-G. Yu, H.-J. Xu and Y. Fu, *Green Chem.*, 2015, **17**, 1038–1046; (*d*) G. S. Zhang, M. M. Zhu, Q. Zhang, Y. M. Liu, H. Y. He and Y. Cao, *Green Chem.*, 2016, **18**, 2155–2164; (*e*) Y. Yang, Z. Du, Y. Huang, F. Lu, F. Wang, J. Gao and J. Xu, *Green Chem.*, 2013, **15**, 1932–1940.

5 (*a*) Z. Yu, Z. Zou, R. Wang, G. Li, A. Wang, Y. Cong, T. Zhang and N. Li, *Angew. Chem., Int. Ed.*, 2023, **62**, e202300008; (*b*) Z. Zou, Z. Yu, W. Guan, Y. Liu, Y. Yao, Y. Han, G. Li, A. Wang, Y. Cong, X. Liang, T. Zhang and N. Li, *Nat. Commun.*, 2024, **15**, 3723.

6 R. Baldenhofer, J.-P. Lange, S. R. A. Kersten and M. P. Ruiz, *ACS Sustainable Chem. Eng.*, 2025, **13**, 681–691.

7 L. Ao, W. Zhao, Y. S. Guan, D. K. Wang, K. S. Liu, T. T. Guo, X. Fan and X. Y. Wei, *RSC Adv.*, 2019, **9**, 3661–3668.

8 Q. Liu, X. Zhang, Q. Zhang, Q. Liu, C. Wang and L. Ma, *Energy Fuels*, 2020, **34**, 7149–7159.

9 W. Wang, X. Ji, H. Ge, Z. Li, G. Tian, X. Shao and Q. Zhang, *RSC Adv.*, 2017, **7**, 16901–16907.

10 (*a*) J. Li, Y. Hao, M. Zhong, L. Tang, J. Nie and X. Zhu, *Dyes Pigm.*, 2019, **165**, 467–473; (*b*) F. Dumur, *Catalysts*, 2023, **13**, 493.

11 W. Wang, S. Y. Sun, F. G. Han, G. Y. Li, X. Z. Shao and N. Li, *Catalysts*, 2019, **9**, 11.

12 S. Shao, W. Dong, X. Li, H. Zhang, R. Xiao and Y. Cai, *J. Cleaner Prod.*, 2020, **250**, 119459.

13 Q. Wang, J. Feng, L. Zheng, B. Wang, R. Bi, Y. He, H. Liu and D. Li, *ACS Catal.*, 2020, **10**, 1353–1365.

14 (*a*) M.-M. Millet, G. Algara-Siller, S. Wrabetz, A. Mazheika, F. Girgsdies, D. Teschner, F. Seitz, A. Tarasov, S. V. Levchenko, R. Schlögl and E. Frei, *J. Am. Chem. Soc.*, 2019, **141**, 2451–2461; (*b*) T. X. Nguyen, J. Patra,

J.-K. Chang and J.-M. Ting, *J. Mater. Chem. A*, 2020, **8**, 18963–18973; (*c*) P. S. Bagus, C. J. Nelin, C. R. Brundle, B. V. Crist, E. S. Ilton, N. Lahiri and K. M. Rosso, *Inorg. Chem.*, 2022, **61**, 18077–18094.

15 (*a*) M. Wang, H. Chen, M. Wang, J. Wang, Y. Tuo, W. Li, S. Zhou, L. Kong, G. Liu, L. Jiang and G. Wang, *Angew. Chem., Int. Ed.*, 2023, **62**, e202306456; (*b*) M. Gao, Z. Wang, Z. Liu, Y. Huang, F. Wang, M. Wang, S. Yang, J. Li, J. Liu, H. Qi, P. Zhang, X. Lu and X. Feng, *Adv. Mater.*, 2023, **35**, 2305575; (*c*) S. Poulston, P. M. Parlett, P. Stone and M. Bowker, *Surf. Interface Anal.*, 1996, **24**, 811–820.

16 X. Zhou, C. Luo, M. Luo, Q. Wang, J. Wang, Z. Liao, Z. Chen and Z. Chen, *Chem. Eng. J.*, 2020, **381**, 122587.

17 M. a. J. Climent, A. Corma, S. Iborra and A. Velty, *J. Mol. Catal. A: Chem.*, 2002, **182–183**, 327–342.